JOURNAL OF MATERIALS SCIENCE 32 (1997) 6039–6047

Physicochemical characterization of WO_3/ZrO_2 and WO_3/Nb_2O_5 catalysts and their photoactivity for 4-nitrophenol photooxidation in aqueous dispersion

C. MARTIN, I. MARTIN, V. RIVES*, G. SOLANA
Dipartamento de Química Inorgánica, Universidad de Salamanca, Facultad de Farmacia, 37007-Salamanca, Spain

V. LODDO, L. PALMISANO, A. SCLAFANI
Dipartimento di Ingegneria Chimica dei Processi e dei Materiali, Universitá di Palermo, Viale delle Scienze, 90128 Palermo, Italy

Two different photo-catalysts consisting of tungsten oxide supported on zirconia and niobia have been studied. The photoactivity of the samples has been investigated in both the absence and presence of H_2O_2 for the photo-oxidation of 4-nitrophenol in aqueous suspensions and compared to that of WO_3 and of the pure ZrO_2 and Nb_2O_5 supports. Both catalysts were found to be photoactive, although no beneficial influence of the presence of tungsten oxide on the reaction rate was observed in the absence of H_2O_2. The presence of hydrogen peroxide was observed to be beneficial for all of the samples. Scanning electron microscopy, X-ray diffraction, diffuse reflectance and laser Raman spectroscopies, surface area and porosity determination, as well as Fourier transform infra-red spectroscopy monitoring of surface acidity were used to characterize the catalysts.

1. Introduction

Tungsten trioxide is a highly selective catalyst for reactions such as the oxidation of benzene and toluene to maleic anhydride and benzaldehyde respectively [1, 2]. It has a high surface acidity [3, 4] and so it is well suited for the olefin metathesis [5] and hydrotreatment reactions [6]. When supported on another metal oxide (i.e., silica, alumina, titania), it exists in a two-dimensional structure, the nature of which can be modified by changing the calcination temperature, preparation method and type of support, which results in the modification of the physicochemical and catalytic properties. These systems have been of considerable interest in the last decade and a significant number of papers have been published in the literature [7–10]. However, data on systems where the tungsten trioxide is supported on niobia and zirconia are scarce in the literature.

In this paper we report on the properties of two catalysts, containing tungsten trioxide supported on zirconia and on niobia. They have been characterized by X-ray diffraction, Raman spectroscopy, the adsorption of nitrogen at low temperature for specific surface area and texture, and Fourier transform infrared spectroscopy (FT-IR) monitoring of pyridine adsorption for surface acidity. The photoactivity has been studied in the photooxidation of 4-nitrophenol in aqueous dispersion [11].

2. Experimental procedure

2.1. Catalyst preparation

Before incorporation of the tungsten trioxide, both support materials, ZrO_2 (Janssen Chemica, p. a.) and Nb_2O_5 (Niobia H4340 hydrated niobia, from Niobium Product Co., Inc.) were calcined overnight in air at 723 K. The tungsten trioxide was incorporated onto the surfaces of the niobia and zirconia by conventional impregnation of the supports with aqueous solutions of ammonium para-tungstate producing samples designated WZr1 and WNb1 containing approximately one monolayer of the supported phase (as calculated from the specific surface area of the support and the size of the WO_3 "molecule" [9]). After impregnation, the solvent was evaporated and the solids were dried overnight at 373 K and calcined in air at 723 K for 2 h.

2.2. Characterization of the catalysts

X-ray diffraction (XRD) patterns were recorded using a Philips PW1070 diffractometer with Ni-filtered

* Author to whom correspondence should be addressed.

0022–2461

Cu-$K\alpha$ radiation ($\lambda = 0.15405$ nm) and interfaced to a DACO-MP data acquisition microprocessor equipped with Diffract/AT software. The specific surface areas were measured by nitrogen adsorption at 77 K using a conventional, pyrex-high vacuum system (residual pressure 10^{-4} Pa); in this case, samples were outgassed *in situ* for 2 h at 400 K prior to the adsorption experiments.

Scanning electron microscopy (SEM) measurements were performed using a Philips microscope, model 505 operating at 25 kV on specimens upon which a thin layer of gold had been evaporated. An electron microprobe used in the energy dispersive mode (EDX) was used to attain quantitative information on the distribution of the tungsten in the specimens.

The laser Raman spectra (LRS) were recorded on a computer-controlled Jobin-Yvon spectrometer (model U-1000). The 514.5 nm line from a Spectra Physics model 165 argon-ion laser was used as the excitation source. The spectra shift was typically of 4 cm^{-1} and laser source powers of *ca.* 20 mW, measured at the samples, were used. The spectra were recorded in the 200–1200 cm^{-1} range. Diffuse reflectance spectra (DRS) were obtained in the 240–600 nm range by using a Varian DMS 90 UV-vis spectrophotometer equipped with quartz cells. $BaSO_4$ was used as a reference. The surface acidity was monitored from the Fourier-transform infrared (FT-IR) spectra recorded after the adsorption of pyridine, using a Perkin-Elmer 16PC spectrometer coupled to a conventional high vacuum system, using specially-designed cells with CaF_2 windows. The procedure was as follows: the solid was compacted to a self-supported disc (1 cm diameter) weighing 50–60 mg which was calcined at 673 K for 2 h in the cell in order to eliminate any organic impurities adsorbed during preparation. The sample was outgassed at 673 K for 2 h at a residual pressure of *ca.* 10^{-3} Pa, and after cooling to room temperature it was equilibrated with pyridine and then outgassed, while the temperature was raised to 673 K. The spectra of the solids were substracted using the software facilities provided by the computer. Only the 1800–1400 cm^{-1} range is shown in the figures, as this is the range where the bands due to adsorbed species are expected.

2.3. Photoreactivity tests

A pyrex batch photoreactor of cylindrical shape containing 0.25 l of aqueous suspension was used. The photoreactor contained ports in its upper section for the inlet and outlet of gases, for sampling and for pH and temperature measurements. A 125 W medium pressure Hg lamp (Helios Italquartz) was immersed within the photoreactor and the photon flux, measured using a UVX digital radiometer, was 13.5 mW cm^{-2}. This was measured by leaning the radiometer against the exterior wall of the photoreactor containing only pure water. Oxygen was continuously bubbled through the suspensions for about 1 h before switching on the lamp and also during the photoreactivity experiments. The amount of catalyst used for all of the experiments was 1.5 $g l^{-1}$, as in this case the photon flux transmitted out of the reactor was negligible, and the initial 4-nitrophenol (from BDH) concentration was 20 $mg l^{-1}$. The initial pH of the suspension was adjusted to 4.5 by the addition of H_2SO_4 (Carlo Erba RPE), and the temperature inside the reactor was *ca.* 300 K. The photoreactivity runs lasted 2.5 h, and the samples were withdrawn at the following times: 0, 10, 30, 60, 90, 120, and 150 min. 5 ml samples were withdrawn from the suspension and the catalyst was separated from the solution by filtration through 0.45 μm cellulose acetate membranes (HA, Millipore) and subsequent centrifugation. Selected experiments were carried out by adding hydrogen peroxide to the reaction suspension. The 4-nitrophenol: H_2O_2 molar ratio was 1:7, corresponding to a H_2O_2 concentration of 2.6×10^{-3} $mol l^{-1}$. The stoichiometric molar ratio needed to completely oxidize 4-nitrophenol is 1:14. The quantitative determination of 4-nitrophenol was performed by measuring its absorption at 315 nm using a Varian DMS 90 UV-vis spectrophotometer.

3. Results and discussion

3.1. Characterization

3.1.1. X-ray diffraction

The XRD patterns of the supports are shown in Fig. 1. For zirconia, all the recorded lines could be assigned to monoclinic and tetragonal phases, after comparison to the standard spectra reported in the ASTM files [12]. Originally the zirconia was mainly monoclinic (although a small tetragonal impurity exists); the crys-

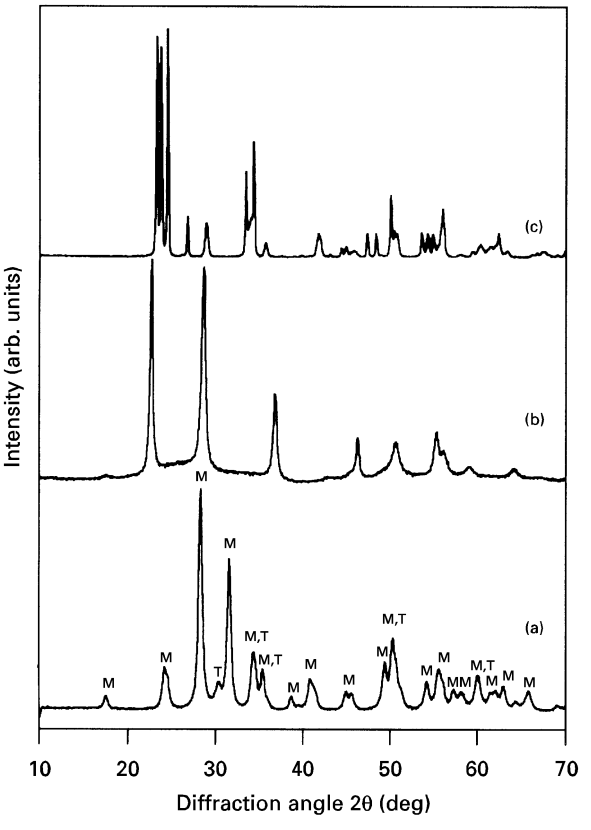

Figure 1 X-ray diffraction patterns of (a) the ZrO_2 support, monoclinic (M) and tetragonal (T) phases, (b) the Nb_2O_5 support and (c) bulk WO_3.

tallographic phase depends on the precursor used to prepare the oxide (gel, salts, etc.), as well as the calcination temperature [13]. The niobia diffraction pattern contained the reflections of the pseudohexagonal phase [14].

The diffraction patterns for samples WZr1 and WNb1 are identical to those of the corresponding supports, i.e., the incorporation of tungsten trioxide does not induce any crystallographic change in the supports. On the other hand, no diffraction peak due

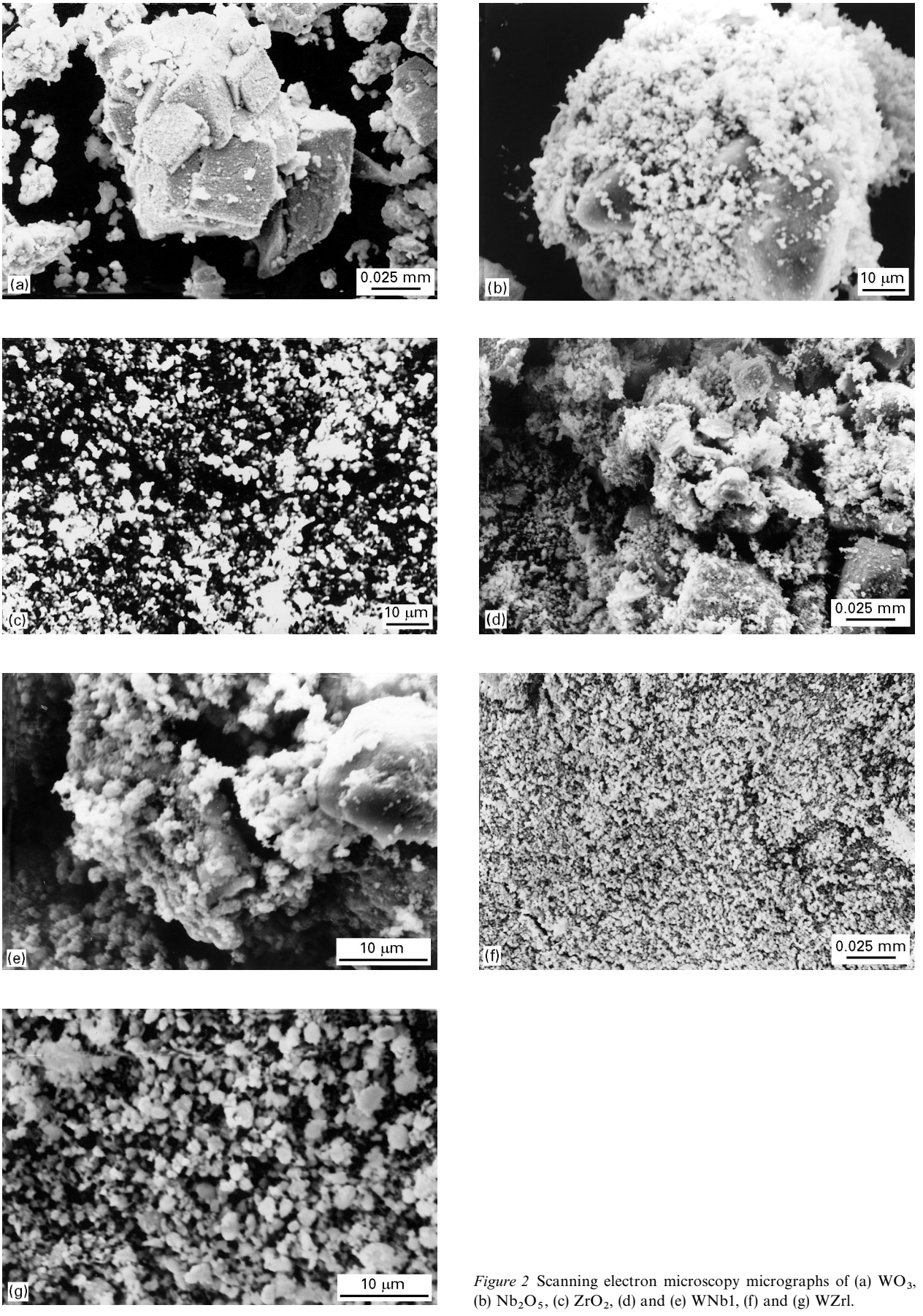

Figure 2 Scanning electron microscopy micrographs of (a) WO_3, (b) Nb_2O_5, (c) ZrO_2, (d) and (e) WNb1, (f) and (g) WZrl.

to tungsten trioxide nor to any tungsten-containing compound is observed, indicating that the supported phase is highly dispersed, probably as tungstates or polytungstates. For comparison purposes, the XRD pattern for WO_3 is also included in Fig. 1.

3.1.2. Scanning electron microscopy

Fig. 2(a–c) are micrographs of the pure WO_3 and the bare Nb_2O_5 and ZrO_2 supports. Fig. 2(d–g) are selected micrographs of samples WNb1 and WZr1.

Large agglomerates of *ca.* 100 μm can be observed for pure WO_3 and Nb_2O_5 samples, that are easily distinguishable from the ZrO_2 sample. The particle size ranges between 1–50 μm for WO_3 and Nb_2O_5, and between 0.5–6 μm for ZrO_2. Similar results are found for the supported samples, which appear to maintain the main features of the corresponding bare supports. In particular, pure ZrO_2 and WZr1 powders show a more uniform distribution of the particle sizes, having almost spherical shapes.

EDX analyses carried out on samples WZr1 and WNb1 indicated a more uniform distribution of tungsten species on the zirconia than on the niobia surface. The figures found were *ca.* 5 at % for WZr1 and 2–7 at % for WNb1, the atomic percentage being calculated as: 100 (moles of W)/(moles of W + moles of Zr or Nb).

TABLE I Specific surface areas ($m^2\ g^{-1}$) and positions (cm^{-1}) of the FT-IR bands recorded after adsorption of pyridine onto the catalysts and supports

Sample	S_{BET}	B_{py}			L_{py}			
		8a	19a	19b	8a	8b	19a	19b
Nb_2O_5	60	1635	1488	1540	1605	1574	1488	1444
ZrO_2	51	—	—	—	1605	1574	1486	1443
WNb1	51	1637	1489	1535	1608	1574	1489	1445
WZr1	44	1638	1489	1538	1609	1574	1489	1446

B_{py} (L_{py}) are the modes corresponding to py adsorbed onto Brønsted (Lewis) acid sites
S_{BET} is the BET derived surface area
8a, 8b, 19a and 19b are vibration modes of the pyridine molecule.

3.1.3. Textural study

Nitrogen adsorption isotherms measured at 77 K for the supports and the samples are shown in Fig. 3. According to the IUPAC classification [15], they all correspond to type IV, and the hysteresis loop corresponds to type H1, which is characteristic of mesoporous substances. The incorporation of tungsten trioxide does not modify the porosity.

The specific surface areas, calculated following the Brunauer–Emmett–Teller (BET) method (see Table 1),

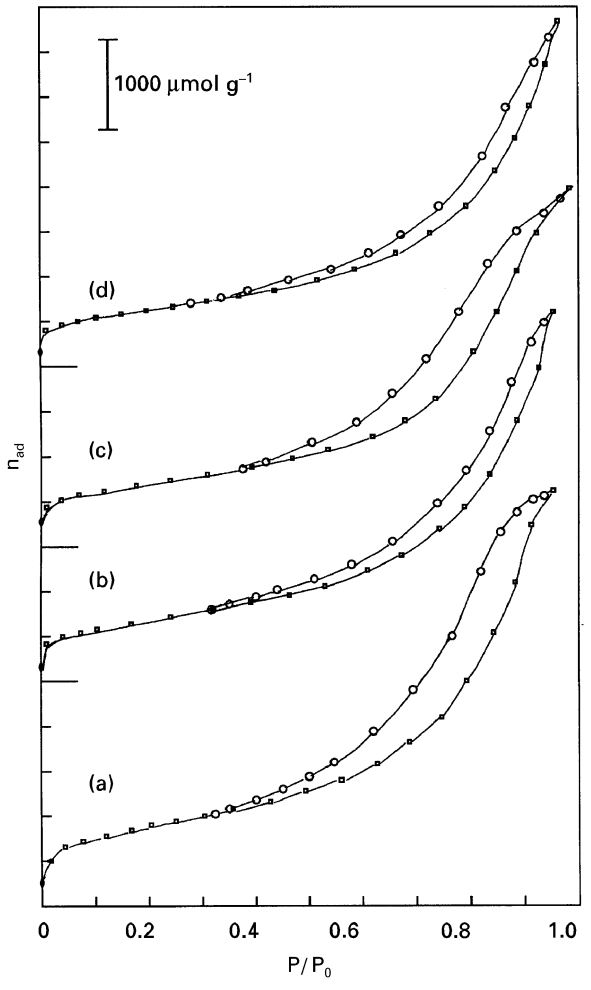

Figure 3 Nitrogen adsorption isotherms measured at 77 K for (●) adsorption and (○) desorption for (a) Nb_2O_5, (b) ZrO_2, (c) WNb1 and (d) WZr1.

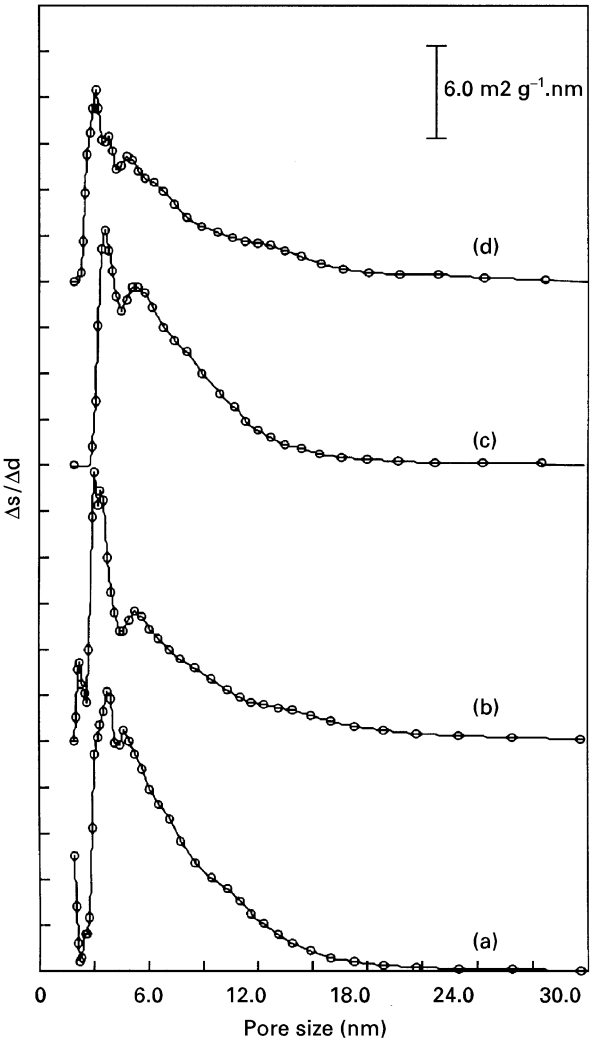

Figure 4 Pore size distribution curves for (a) Nb_2O_5, (b) ZrO_2, (c) WNbl and (d) WZr1.

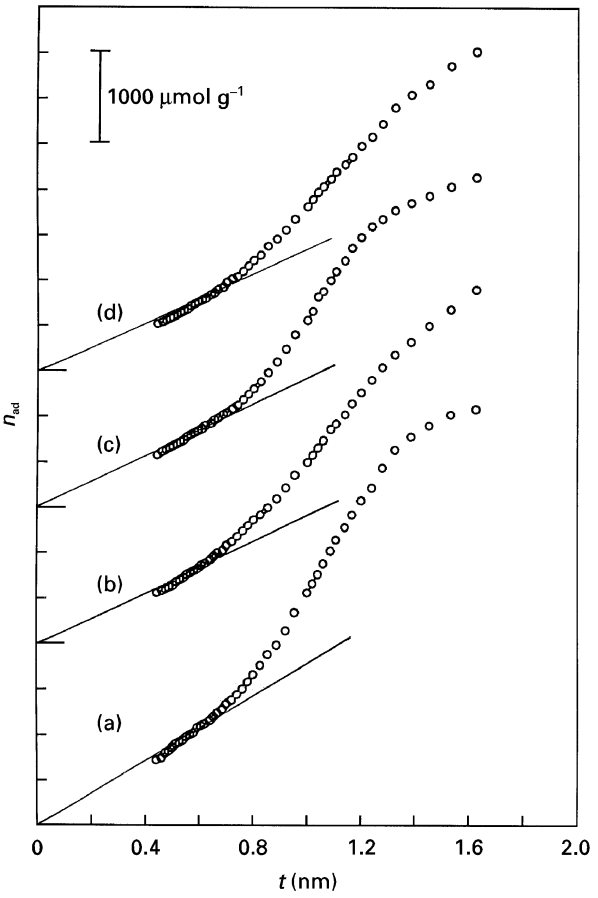

Figure 5 *t*-plots for (a) Nb_2O_5, (b) ZrO_2, (c) WNb1 and (d) WZr1.

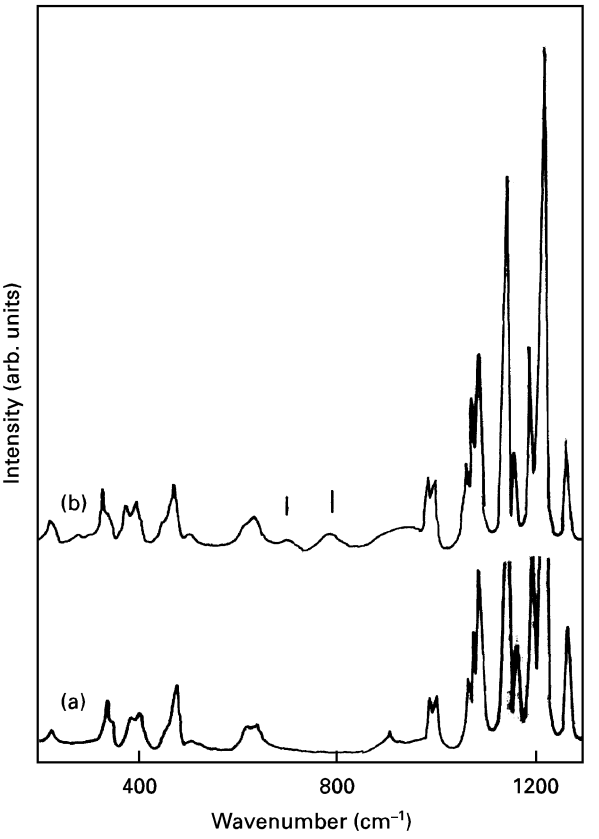

Figure 6 Laser Raman spectra of (a) ZrO_2 support and (b) WZrl.

indicate that the incorporation of the tungsten trioxide leads to a slight decrease in the specific surface areas, amounting to *ca.* 10% for sample WZr1, and 20% for sample WNb1, probably because of a sintering process. The pore size distribution curves shown in Fig. 4 confirm the mesoporosity of all four samples, a maximum contribution to the surface area arising from pores with diameters ranging between 4–8 nm. The absence of micropores in these samples is finally concluded from the *t*-plots [16] in Fig. 5, since extrapolation of the almost-straight segment for low thickness values of the adsorbed layer passes through the origin in all cases. Deviations from linearity at large thickness values is in agreement with the presence of large mesopores [17]. In addition, values calculated for the external surface areas from the *t*-plots coincide with the values calculated following the BET method.

3.1.4. Laser Raman spectroscopy

The laser Raman spectra of the Nb_2O_5 support and of sample WNb1 are coincident. However, for the ZrO_2 support and sample WZr1, some differences are found as can be observed in Fig. 6. In addition to the Raman peaks of the support, sample WZr1 shows two weak, but detectable, peaks at 699 and 805 cm^{-1}. For an ideal, undistorted, $[WO_6]$ octahedron, three Raman active modes are expected, ν_1 (A_{1g}), ν_2 (E_g) and ν_5 (T_{2g}) [18], but in most of the solids containing this species it is distorted, and the symmetry decrease associated with the distortion leads to the activation of previously forbidden modes. Crystalline WO_3 has the ReO_3-type structure [19, 20] and shows intense Raman bands at 805, 706 and 273 cm^{-1}; the first two bands are ascribed to W–O stretching modes, while the third one corresponds to a W–O–W bending mode [21]. For other compounds containing octahedral $[WO_6]$ species (e.g., Li_6WO_6, $CoWO_4$ and H_2WO_4), the higher wavenumber bands are recorded in the 740–980 cm^{-1} range [22], but most of them are below 910 cm^{-1}. On the contrary, in low-distorted tetrahedral $[WO_4]$ species, four bands are recorded, corresponding to the modes $\nu_1(A_1)$, $\nu_2(E)$, $\nu_3(T_2)$ and $\nu_4(T_2)$ [18]; as expected, the number of bands increases upon distortion in the solid state, but in all the compounds containing tetrahedral $[WO_4]$ species ($CaWO_4$, Na_2WO_4) the bands are recorded above 910 cm^{-1} [22]. According to these data, we can conclude that no tetrahedral $[WO_4]$ species exist in sample WZr1, since the recorded positions of all bands, in addition to those of the support, coincide with those of orthorhombic WO_3 containing octahedral $[WO_6]$ species.

3.1.5. Diffuse reflectance spectroscopy

The diffuse reflectance spectra of the bare supports and of the doped samples, as well as that of bulk WO_3, are included in Fig. 7. The absorption from *ca.* 500–300 nm (depending on the material itself) towards lower wavelengths corresponds to the absorption edge of the solids, and should originate in all cases from a $O^{2-} \rightarrow M^{n+}$ charge transfer process from the valence band (mainly 2p orbitals of the oxide anions) to the conduction band, formed by the valence orbitals of

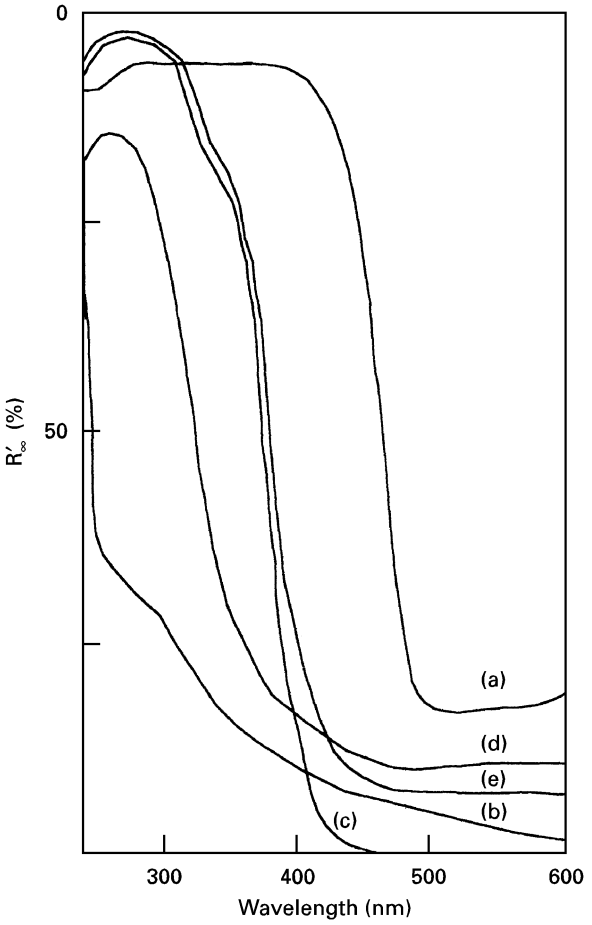

Figure 7 Diffuse reflectance spectra of (a) WO_3, (b) ZrO_2, (c) Nb_2O_5, (d) WZr1 and (e) WNb1.

the cations. It can be noticed that WO_3 absorbs more significantly than both the bare supports and the two doped samples. For sample WZr1, a shoulder at 256 nm is recorded, in addition to those due to the support; this band can be ascribed to a $O^{2-} \rightarrow W^{6+}$ charge transfer process. For H_2WO_4, containing octahedral [WO_6] species, two bands have been reported [7] at 204 and 270 nm. Contrary to the findings for sample WZr1 and the ZrO_2 support, the spectrum recorded for WNb1 closely matches that of the bare Nb_2O_5 support. As expected, the presence of tungsten species on the surface of both doped catalysts enhances their absorption properties, although the effect is less significant for WNb1.

3.1.6. FT-IR monitoring of the surface acidity via pyridine adsorption

Although FT-IR spectroscopy is mainly a qualitative tool to investigate surface sites in polycrystalline oxides, the study of the adsorption of probe molecules provides indirect information about such surface sites and on their chemical properties. This is due to the measurement of changes in the spectroscopic parameters sensitive to the type of bonding between the surface sites and the adsorbed molecules. The adsorption of basic molecules (ammonia and pyridine) provides information about the surface acidity [23, 24], which usually depends on the preparation method, presence of impurities and type of the support.

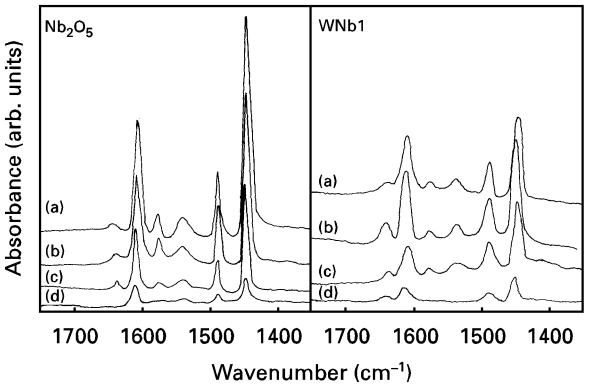

Figure 8 FT-IR spectra recorded after the adsorption of pyridine onto Nb_2O_5 and WNb1 and outgassing at temperatures of (a) room temperature, (b) 373 K, (c) 573 K and (d) 673 K.

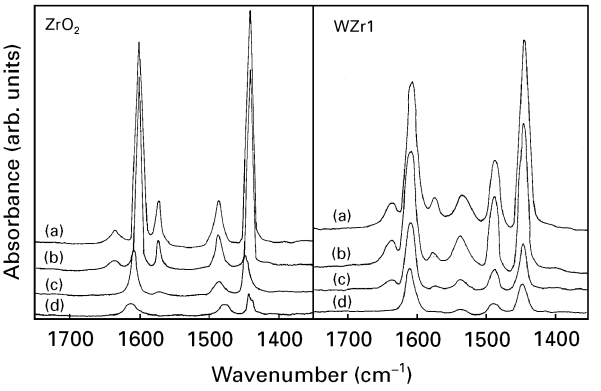

Figure 9 FT-IR spectra recorded after the adsorption of pyridine onto ZrO_2 and WZr1 and outgassing at temperatures of (a) room temperature, (b) 373 K (c) 573 K and (d) 673 K.

The spectrum recorded after the adsorption of pyridine on the Nb_2O_5 support previously outgassed *in situ* as previously described, and outgassing at room temperature is shown as Fig. 8. We can observe bands at 1635, 1605, 1574, 1540, 1488 and 1444 cm^{-1}, that can be ascribed to stretching modes of pyridine, both co-ordinated (i.e., attached to surface Lewis acid sites) and protonated (pyridinium ion), indicating the presence of surface Brønsted acid sites (Table 1). After outgassing at increasing temperatures (Fig. 8) the intensities of the bands decrease, but they are still recorded even after outgassing at 573 K, thus indicating rather strong acid sites. The series of spectra recorded for sample WNb1 submitted to the same treatments (also shown in Fig. 8) are rather similar; the only difference is that the bands are slightly broader and weaker, although this weakness can be due to a poorer transmission of the sample.

The spectrum recorded after adsorption of pyridine on the ZrO_2 support is shown as Fig. 9. We only observe bands at 1605, 1574, 1486, and 1443 cm^{-1}, due to pyridine co-ordinated to surface Lewis acid sites (Table 1), and no band is recorded that could be ascribed to surface Brønsted sites. The sites are also rather strong, as the bands are recorded even after outgassing the sample at 573 K. However, after incorporation of tugsten trioxide to the ZrO_2 support to yield sample WZr1, the spectrum is rather different,

with bands at 1638, 1609, 1574, 1538, 1489, and 1446 cm^{-1} due to both surface Lewis and Brønsted acid sites (Table 1), i.e., the incorporation of tungsten trioxide on the surface of zirconia has led to the development of surface Brønsted acid sites. When the sample is outgassed at increasing temperatures, all the bands remain even after outgassing at 673 K, thus indicating that strong Lewis and Brønsted acid sites exist on the surface of this sample.

3.1.7. Photoreactivity

Photodegradation of the three isomers of nitrophenol has been recently extensively studied in aqueous suspensions employing polycrystalline TiO_2 (anatase) as a photocatalyst. The degradation process exhibited pseudo-first order kinetics with respect to the organic substrate concentration [11, 25]. In this work, 4-nitrophenol photodegradation has been used only as a probe reaction and it is not the aim of this paper to deal with the mechanistic and kinetic aspects of the reaction.

The experimental results fitted a pseudo-first order kinetics with respect to the organic substrate concentration which can be expressed as:

$$-\mathrm{d}C/\mathrm{d}t = k_{\mathrm{obs}}\, C \qquad (1)$$

where C stands for the 4-nitrophenol concentration, k_{obs} for the observed pseudo-first order rate constant and t for the time.

The values for the observed pseudo-first order rate constants, as measured both in the absence and presence of hydrogen peroxide in the reaction medium, are given in Table II for bulk tungsten trioxide, the supports and the catalysts. Representative results are also presented in Fig. 10.

The observed pseudo-first order rate constant values (k_{obs}) indicate that WNb1 is more photoactive than WZr1, although the reaction rates are rather low for both samples. Moreover, the photoactivities of both samples do not significantly change, if compared to that of the corresponding bare support, and they are also lower than that of pure polycrystalline WO_3. It is noteworthy, however, that the reaction rates for all of the pure and doped samples are far lower than that of pure polycrystalline commercial (Merck) titania (anatase) samples ($k_{\mathrm{obs}} = 6 \times 10^{-4}\ s^{-1}$ under the same experimental conditions). The different photoactivities of the pure oxides, and in particular the higher photoactivity of WO_3, can be explained by considering the band-gap values (2.6, 5.0 and 3.4 eV for WO_3, ZrO_2, and Nb_2O_5, respectively [26]), and the emission spectrum of the lamp, although it is well known [27] that several other physico-chemical and electronic factors can play a role in determining the level of photoreactivity. The photoexcitation of WO_3 can occur by using light with wavelengths ranging approximately between 300–480 nm (check Fig. 7), as the walls of the pyrex photoreactor cut off all the radiation with a wavelength lower than 300 nm, and only *ca.* 47% of the energy emitted by the lamp can be used, taking into account its emission spectrum.

TABLE II Observed rate constants in the absence (k_{obs}) and presence (k'_{obs}) of H_2O_2 for photo-oxidation of 4-nitrophenol*

Sample	k_{obs} ($10^5\ s^{-1}$)	k'_{obs} ($10^5\ s^{-1}$)
WO_3	9.3	12.3
ZrO_2	1.3	1.9
Nb_2O_5	4.7	7.4
WZr1	1.3	2.9
WNb1	4.6	6.8

* H_2O_2 : 4-nitrophenol = 1 : 7 molar ratio

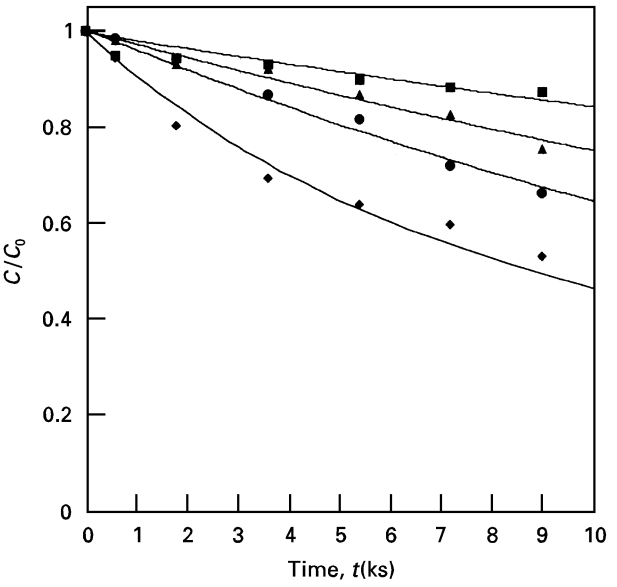

Figure 10 Change in the relative concentration of 4-nitrophenol as a function of time during photo-oxidation in the absence of H_2O_2 for (■) WZr1 and (●) WNb1 and the presence of H_2O_2 for (▲) WZr1 and (◆) WNb1. (C_0 is the initial concentration).

Niobia can be photoexcited by light with a wavelength ranging between 300–410 nm (see Fig. 7), and only *ca.* 27% of the total energy emitted by the lamp can be utilized. This last value corresponds to 58% of the fraction that can be utilized by WO_3 and, consequently, at least for the range of energy used in this work, the photocatalytic activity of niobia can be considered not too much different from that of WO_3.

With regards to bare zirconia, its expected photoactivity, under the experimental conditions used and taking into account the filtering effect of the pyrex walls and data for zirconia in Fig. 7, should be negligible. The observed activity could even be the result of a photochemical homogeneous reaction and/or partial oxidation of the adsorbed substrate by direct interaction with photons [28]. The diffuse reflectance spectrum reported in Fig. 7 indicates that some light absorption by the solid occurs in the range 400–300 nm, probably due to the presence of surface states and, consequently, the occurrence of heterogeneous photooxidation processes cannot be excluded. It should also be noted that absorption in the same range has been reported for thin anodic films grown on metallic zirconium [29, 30]. The characterization results (XRD, SEM and specific surface area measurements) indicate that the presence of WO_3 did not substantially modify the crystalline habit and the morphology of

the supports. The FT-IR results indicate that the acid-base properties of niobia were not modified, while some Brønsted acid sites developed in zirconia. The photoreactivity experiments confirmed the above insights, since the presence of highly dispersed microcrystalline and/or amorphous tungsten trioxide species on the surface, although giving rise to a modification of the absorption properties of both supports, does not influence their photoactivity. A different behaviour was shown, however, by mixed tungsten trioxide–titanium dioxide samples [31].

If hydrogen peroxide is present in the reacting suspensions, the photoreactivity is higher for all of the specimens. The positive influence of hydrogen peroxide on the reaction rate is well known when pure titania is used as a photocatalyst [32–34]. The enhancement of the photoactivity observed in the presence of H_2O_2 for suspensions containing WZr1 can also be explained by considering that H_2O_2 (with a higher oxidizing ability than molecular oxygen), can mainly enhance the rate of the homogeneous reaction. For WNb1, the photocatalytic activity in the presence of H_2O_2 was similar to that shown by Nb_2O_5, for which a more significant enhancement of the reaction rate occurred and the mechanistic aspects of the heterogeneous photoprocesses could be very similar to those proposed for TiO_2 [11, 25]. As can also be noticed from Fig. 10, the presence of tungsten trioxide on zirconia and niobia surfaces did not substantially modify the photoactivity of the supports in both the absence and presence of hydrogen peroxide.

4. Conclusions

The results obtained in this work indicate that samples WZr1 and WNb1 are mesoporous, as the original supports were, although a 10–20% decrease in the specific surface area (sintering) takes place after the incorporation of the tungsten trioxide, without any change in the crystallographic phases of the supports. The supported phases are highly dispersed, since they give rise to no diffraction line in the XRD patterns. Raman spectroscopy indicates that the oxo-tungsten species in sample WZr1 are octahedral, $[WO_6]$, similar to those existing on orthorhombic WO_3 (distorted ReO_3 structure). Both tungsten trioxide-containing samples exhibit strong surface Lewis and Brønsted acid sites, larger than in the original supports, due to the presence of W^{6+} containing species, leading to highly covalent W–O bonds. Consequently, the content of Brønsted acidic WO–H groups and poorly basic W–O–W bridging units increases.

No significant effect is observed after the dispersion of the tungsten trioxide on the surface of niobia or zirconia on the photo-oxidation of 4-nitrophenol in the absence or presence of hydrogen peroxide.

Acknowledgements

V. L., L. P. and A. S. thank Ministero dell'Universitá e della Ricerca Scientifica e Tecnologica (MURST, Italy), and C. M., I. M., V. R. and G. S. thank Dirección General de Investigación Científica y Técnica (PB93–633, Spain) for financial support. G. S. also acknowledges a leave of absence from the Universidad de Guanajuato (México).

References

1. J. HABER, J. JANAS, M. SCHIAVELLO and R. J. D. TILLEY, *J. Catal.* **82** (1983) 395.
2. W. T. A. HARRINSON, U. CHOWDRY, C. J. MACHIELS, A. W. SLEIGHT and A. K. CHEETHAM, *J. Solid State Chem.* **82** (1985) 101.
3. S. L. SOLED, G. B. McVICKER, L. L. MURRELL, L. G. SHERMAN, N. C. DISPENZIERE, S. L. SHU and D. WALDMAN, *J. Catal.* **111** (1988) 286.
4. G. RAMIS, G. BUSCA and V. LORENZELLI, in "Structure and reactivity of surfaces", edited by C. Morterra, A. Zecchina and G. Costa (Elsevier, Amsterdam, 1989) p. 777.
5. J. C. MOL and J. A. MOULIJN, in "Catalysis, science and technology", edited by J. R. Anderson and M. Boundart Springer Verlag, Berlin, 1987.
6. D. C. McCULLOCH, in "Applied industrial catalysis", Vol. 1, edited by B. E. LEACH (Academic Press, New York, 1983) p. 69.
7. A. IANNIBELLO, S. MARENGO and P. TITTARELLI, *J. Chem. Soc., Faraday Trans. I* **80** (1984) 2209.
8. F. MAUGÉ, J. P. GALLAS, J. C. LAVALLEY, G. BUSCA, G. RAMIS and V. LORENZELLI, *Mikrochim. Acta* **11** (1988) 57.
9. D. C. VERMARIE and P. C. van BERGE, *J. Catal.* **116** (1989) 309.
10. R. L. BRADY, D. SOUTHMAYD, C. CONTESCU, R. ZHANG and J. A. SCHWARZ, *ibid.* **129** (1991) 195.
11. V AUGUGLIARO, L. PALMISANO, M. SCHIAVELLO, A. SCLAFANI, L. MARCHESE, G. MARTRA and F. MIANO, *Appl. Catal.* **69** (1991) 323.
12. ASTM Powder Diffraction Files, cards no. 17-923 and 37-1484.
13. M. A. VILLA GARCÍA, M. C. FERNÁNDEZ and C. OTERO AREÁN, *Thermochim. Acta* **126** (1988) 33.
14. ASTM Powder Diffraction Files, card. no. 7-061.
15. K. S. W. SING, R. A. W. HAUL, L. MOSCOU, R. A. PIEROTTI, J. ROUQUEROL and T. SIEMINIEWSKA, *Pure Appl. Chem.* **57** (1985) 603.
16. B. C. LIPPENS and J. H. de BOER, *J. Catal.* **4** (1965) 319.
17. J. C. P. BROEKHOFF and B. G. LINSEN, in "Physical and chemical aspects of adsorbents and catalysts", edited by B. G. Linsen (Academic Press, New York, 1970) p. 1.
18. N. NAKAMOTO, "Infrared and Raman spectra of inorganic and co-ordination compounds" (Wiley, New York, 1978).
19. M. F. DANIEL, B. DESBART, J. C. LASSEGUES, B. GERAND and M. FLIGLARZ, *J. Solid State Chem.* **67** (1987) 235.
20. G. RAMIS, C. CRISTIANI, A. S. ELMI and R. VILLA, *J. Molecular Catal.* **61** (1990) 319.
21. I. R. BEATTIE and T. R. GILSON, *J. Chem. Soc. A* (1969) 2322.
22. J. A. HARSLEY, I. E. WACHS, J. M. BROWN, G. H. VIA and F. D. HARDCASTLE, *J. Phys. Chem.* **91** (1987) 4014.
23. H. KNÖZINGER, *Adv. Catal.* **25** (1976) 184.
24. H. A. BENES and B. H. C. WINQUIST, *ibid.* **27** (1978) 97.
25. V. AUGUGLIARO, M. J. LÓPEZ-MUÑOZ, L. PALMISANO and J. SORIA, *Appl. Catal. A General* **101** (1993) 7.
26. S. R. MORRISON, "Electrochemistry at semiconductor and oxidation metal electrodes" (Plenum Press, New York, 1980) p. 183.
27. M. SCHIAVELLO, *Electrochim. Acta* **38** (1993) 11.
28. M. SCHIAVELLO, V. AUGUGLIARO, S. COLUCCIA, L. PALMISANO and A. SCLAFANI, in "Photochemistry on solid surfaces", edited by M. Anpo and T. Matsuura (Elsevier, Amsterdam, 1989) p. 149.
29. P. MEISTERJAHN, H. W. HOPPE and J. W. SCHULTZE, *J. Electroanal. Chem.* **217** (1989) 159.

30. F. DI QUARTO, S. PIAZZA, C. SUNSERI, in "Modification of passive films", edited by P. Marcus, B. Baroux and M. Keddam (The Institute of Materials, Paris, 1994) p. 76.
31. G. MARCÍ, L. PALMISANO, A. SCLAFANI, A. M. VENEZIA, R. CAMPOSTRINI, G. CARTURAN, C. MARTIN, I. MARTIN and V. RIVES, *J. C. S. Faraday Trans.* **92** (1996) 819.
32. V. AUGUGLIARO, E. DAVÌ, L. PALMISANO, M. SCHIAVELLO and A. SCLAFANI, in "Environmental contamination", edited by A. A. Orio (CEP Consultants, Edinburgh, 1988) p. 206.
33. K. TANAKA, T. HISANAGA and K. HARADA, *New. J. Chem.* **13** (1989) 5.
34. V. AUGUGLIARO, E. DAVÍ, L. PALMISANO, M. SCHIAVELLO and A. SCLAFANI, *Appl. Catal.* **60** (1990) 101.

Received 25 March
and accepted 19 December 1996